Banner appropriate to article type will appear here in typeset article

Bouncing to coalescence transition for droplet impact onto moving liquid pools

Daniel M. Harris¹, Luke F.L. Alventosa¹, Oliver Sand¹, Eli Silver¹, Arman Mohammadi¹, Thomas C. Sykes^{2,3}, Alfonso A. Castrejón-Pita³, and Radu Cimpeanu⁴

- ¹ School of Engineering, Brown University, Providence, RI 02912, USA
- ² School of Engineering, University of Warwick, Coventry CV4 7AL, UK
- ³ Department of Engineering Science, University of Oxford, Oxford OX1 3PJ, UK
- ⁴ Mathematics Institute, University of Warwick, Coventry CV4 7AL, UK

Corresponding author: Daniel M. Harris, daniel_harris3@brown.edu

(Received xx; revised xx; accepted xx)

A droplet impacting a deep fluid bath is as common as rain over the ocean. If the impact is sufficiently gentle, the mediating air layer remains intact, and the droplet may rebound completely from the interface. In this work, we experimentally investigate the role of translational bath motion on the bouncing to coalescence transition. Over a range of parameters, we find that the relative bath motion systematically decreases the normal Weber number required to transition from bouncing to merging. Direct numerical simulations demonstrate that the depression created during impact combined with the translational motion of the bath enhances the air layer drainage on the upstream side of the droplet, ultimately favoring coalescence. A simple geometric argument is presented that rationalizes the collapse of the experimental threshold data, extending what is known for the case of axisymmetric normal impacts to the more general 3D scenario of interest herein.

1. Introduction

When two volumes of fluid approach one another in a gas, whether they be droplets, jets, or a droplet and a bath, the outcome of the impact is determined by the properties and persistence of a thin interstitial gas layer (Rein 1993; Neitzel & Dell'Aversana 2002; Yarin 2006; Sprittles 2024). For relatively low-energy collisions in air, the liquids may rebound completely from one another having never made direct contact, provided the inertia of the liquid is insufficient to drain the air layer during the interaction. The critical role of the air layer was first hypothesized by Lord Rayleigh for the case of colliding jets, similarly framing the essential question as to "...whether the air can be anywhere squeezed out during the short time over which the collision extends" (Rayleigh 1899). More specifically, the air layer must drain to a sufficient thickness such that van der Waals forces can initiate coalescence, a length scale typically on the order of $0.1~\mu m$ (Couder *et al.* 2005; Tang *et al.* 2019; Sprittles 2024).

In the present work, we focus on the bouncing to coalescence (BC) transition for the case of a droplet impacting a deep planar bath, first examined in the seminal contribution of Schotland (1960). Schotland identified the transition between rebound and coalescence for a continuous stream of droplets impacting a fluid bath at an oblique angle. They noted that for a fixed liquid and gas pair, the transition between rebound and coalescence was principally dictated by the normal Weber number, defined as

$$We = \frac{\rho V^2 R}{\sigma},\tag{1.1}$$

where ρ is the fluid density, V is the droplet impact velocity projected normal to the undisturbed bath interface, R is the droplet radius, and σ is the surface tension (Figure 1(a)). The bouncing to coalescence transition was further interrogated for oblique streams of droplets in numerous follow-up works (Jayaratne & Mason 1964; Ching *et al.* 1984; Zhbankova & Kolpakov 1990; Doak *et al.* 2016), where it has continued to be accepted that the BC transition (for a given set of fluids) is governed by the normal Weber number, with the relative tangential motion of immaterial consequence.

Single droplets may also rebound from a quiescent fluid bath, with the bouncing to coalescence transition occurring above a critical Weber number that depends on the liquid and gas properties (Rodriguez & Mesler 1985; Pan & Law 2007; Huang & Zhang 2008; Zhao et al. 2011; Zou et al. 2011; Tang et al. 2016, 2018; Wu et al. 2020; Wu & Saha 2022). Although the depth (H) of the fluid bath also plays a critical role in determining the outcome when it is on the order of the droplet size (Pan & Law 2007), our focus here is on the case of deep baths where $H \gg R$. Despite the considerable progress over the last several decades, these prior works have focused exclusively on the axisymmetric case of normal droplet impacts on a still fluid bath. At this point it remains unknown what role tangential motion might play in determining the transition between bouncing and coalescence, and in particular, if the normal Weber number is sufficient to determine the outcome. Herein we experimentally demonstrate that relative bath motion leads to a systematic reduction in the critical normal Weber number, in contrast to other scenarios where relative substrate motion has been shown to favor non-coalesce behavior (Neitzel & Dell'Aversana 2002; Che et al. 2015; Castrejón-Pita et al. 2016; Gauthier et al. 2016; Sprittles 2024). Companion threedimensional direct numerical simulation results allow us to interrogate the air layer dynamics during impact and isolate the mechanism responsible for the reduction.

2. Experimental methods

2.1. Experimental setup

A rendering of the experimental setup is shown in Figure 1(b). Droplets of silicone oil are generated from a piezoelectric droplet-on-demand generator (Harris *et al.* 2015; Ionkin & Harris 2018) and impact a fluid bath of the same fluid. The working fluids are silicone oil (Clearco Products) with kinematic viscosities $v = \mu/\rho = 2$, 20, and 50 cSt. These fluids correspond (respectively) to densities of $\rho = 0.873$, 0.949, 0.960 g/cm³ and surface tension coefficients of $\sigma = 18.7$, 20.6, and 20.8 dynes/cm, as provided by the manufacturer datasheet. The latest version of the generator, and the one employed for this work, is documented at https://github.com/harrislab-brown/DropGen. Interchangeable nozzles allow for control of the droplet radius - commercial 3D-printer nozzles of outlet diameter 0.3, 0.5 and 1.0 mm are used in the present work, resulting in droplet sizes ranging from R = 0.2 - 0.4 mm. The fluid and droplet sizes used correspond to Bond numbers ($Bo = \rho g R^2/\sigma$) ranging from 0.01 to 0.09 and Ohnesorge numbers

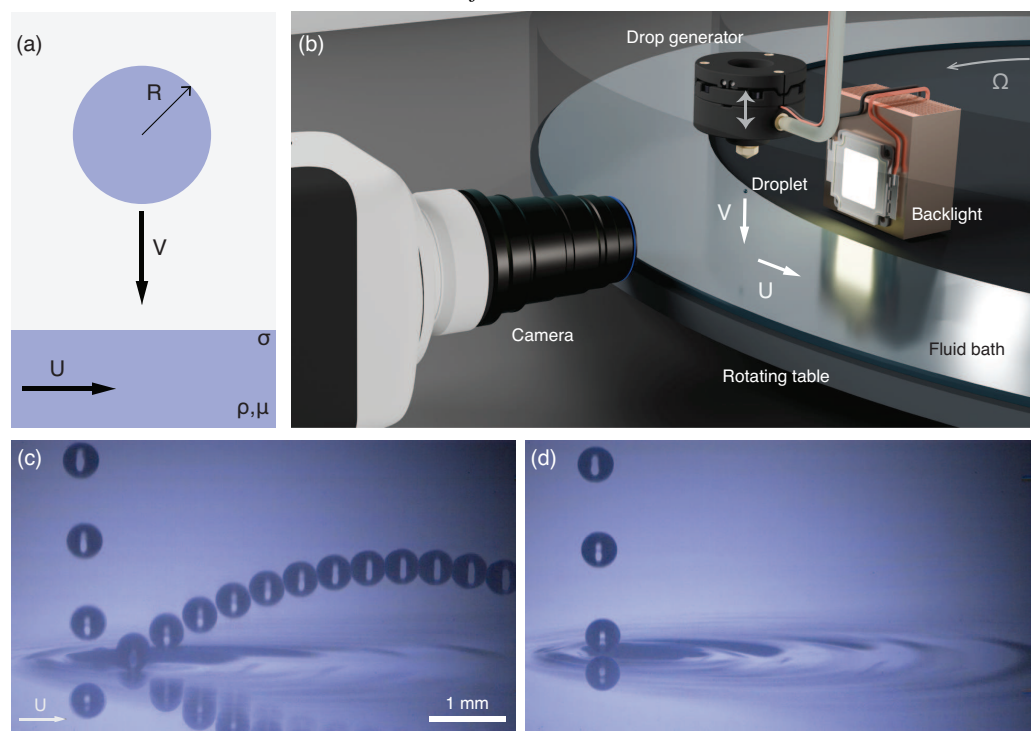


Figure 1. (a) Schematic of a droplet impacting a moving bath of the same fluid. (b) Rendering of experimental setup. A droplet is generated by a piezoelectric droplet generator and impacts a moving fluid layer atop a rotating table. The dynamics are filmed from the side with a high-speed video camera. (c,d) A 2 cSt silicone oil droplet of radius $R = 0.230 \pm 0.006$ mm impacts a fluid bath moving with horizontal speed U = 35 cm/s. Images spaced by 1/540 seconds are directly superimposed. (c) With an impact velocity of $V = 59.3 \pm 0.9$ cm/s, the droplet rebounds from the fluid bath while obtaining a horizontal velocity from the bath during contact. (d) At $V = 60.7 \pm 0.8$ cm/s, the droplet merges with the bath and the residual interfacial disturbance is transported downstream following coalescence. Corresponding Videos available in Supplementary Movie 1.

 $(Oh = \mu/\sqrt{\rho\sigma R})$ ranging from 0.02 to 0.5, suggesting that gravity and viscosity play a secondary role with the dynamics dominated by inertia and capillarity (Alventosa *et al.* 2023). The droplet generator head is mounted on a vertically oriented motorized translation stage controlled by a stepper motor that allows for vertical displacement of the generator (with resolution of 1280 steps per mm) in order to vary the droplet impact velocity, and therein the Weber number.

Horizontal motion of the liquid bath is achieved via a large rotating table, with design and construction inspired by the 'Weather in a Tank' apparatus (Illari $et\ al.\ 2009$). The rotating circular platform has a diameter of 0.71 m and is driven into steady rotation at speeds up to $\Omega=10$ rpm by a friction wheel. The fluid is confined within an annulus with inner diameter 0.61 m surrounded on either side by thin clear walls of height 7.6 cm and thickness 4.7 mm. A similar rotating annular bath setup has been used in prior work to study the rebound of vertical fluid jets impacting a translating fluid bath (Thrasher $et\ al.\ 2007$). The annulus is filled with 1 liter of silicone oil corresponding to a mean fluid depth of 4.5 mm. Prior work has demonstrated that depths greater than approximately 2-3 droplet radii correspond to deep-bath limit for the bouncing to coalescence threshold (Pan & Law 2007; Tang $et\ al.\ 2018$; Wu & Saha 2022), the regime of interest for the present work. The droplet generator is positioned such that each droplet impacts at the center of the

annular region. Bath linear translation speeds (as evaluated at the impact location) of up to $U=35\,\mathrm{cm/s}$ are achieved with the design and explored in the present work. The speed is monitored by an encoder attached to a second spring-loaded friction wheel and held constant via closed-loop feedback control. Maximum uncertainty in the bath speed U at the impact position was estimated to be 2% of the reported value. Inevitably, the table rotation leads to a curved parabolic interface shape in steady state. At the maximum speed used in the present work, the interface has an estimated 2.2° inward slope at the impact location. The annular bath is covered when not in use to minimize ambient contamination.

The dynamics are imaged through the outer annulus with a high-speed video camera (Phantom Miro LC 311) and macro lens (Laowa 25 mm Ultra Macro) at a frame rate of 15,000 frames per second, exposure time of 50 μ s, and spatial resolution of 7.8 μ m per pixel. The droplet and bath are illuminated using a custom LED backlight. To clearly view the droplet and bath interface in all cases the camera is angled downward at 8°, leading to small errors on distances and speeds of no more than 1%. A transition from bouncing to coalescence following a slight increase in V is shown in Figure 1(c,d).

2.2. Experimental procedure

To start an experiment, the bath is set at the desired linear speed and left to equilibrate for several minutes before experiments are performed. Droplets are then generated at a frequency of 2 Hz or slower. The generator is positioned sufficiently high such that all droplets coalesce. The generator is then lowered by 1.0 mm and 15 successive droplet impacts are observed. The lowering process is repeated until at least 13 of 15 of the observed droplets rebound, at which point a single video recording is taken for droplet size and velocity measurements. The generator is then raised by 1.0 mm until 13 of 15 droplets coalesce, and another video is taken. This process (incremental lowering/raising) is repeated twice more before moving to a new table speed. After surveying all table speeds, the overall procedure is repeated twice more for a total of three times. This protocol results in a total of nine measurements of the bouncing threshold and nine measurements of the coalescence threshold at each table speed. The transition between regimes occurs over a relatively narrow range of impact velocities, typically on the order of 2 cm/s. The video recordings are post-processed in MATLAB using Canny edge detection to obtain the droplet radius and velocities as detailed in prior work (Alventosa *et al.* 2023).

3. Direct numerical simulation

Complementing the experimental setup deployed in this study, we have developed a three-dimensional numerical counterpart using the open-source software Basilisk (Popinet 2009, 2015), which has been successfully used for studying bouncing phenomena recently (Alventosa *et al.* 2023; Sanjay *et al.* 2023; Ray *et al.* 2024; Phillips *et al.* 2025). Our multiscale setup, balancing the requirement to resolve the thin gas film entrapped between the impacting drop and the moving pool, with a sufficiently large scale domain to ensure the rebound is unaffected by finite size effects, make it an ideal candidate for the adaptive mesh refinement and parallelization features of the code. The full implementation is made available at https://github.com/rcsc-group/BouncingDropletsMovingPool3D. The domain construction builds on a computational box measuring 20^3 dimensionless units (relative to a dimensionless impacting drop radius of 1), making use of the one viable symmetry plane (the x-z plane), and is illustrated in Figure 2(a). This choice ensures that outward propagating waves have sufficient space to develop and exit the domain cleanly. The droplet is initialized with its south pole one radius above the pool, and a uniform imposed vertical velocity field within. Gravitational effects are also included in the simulation

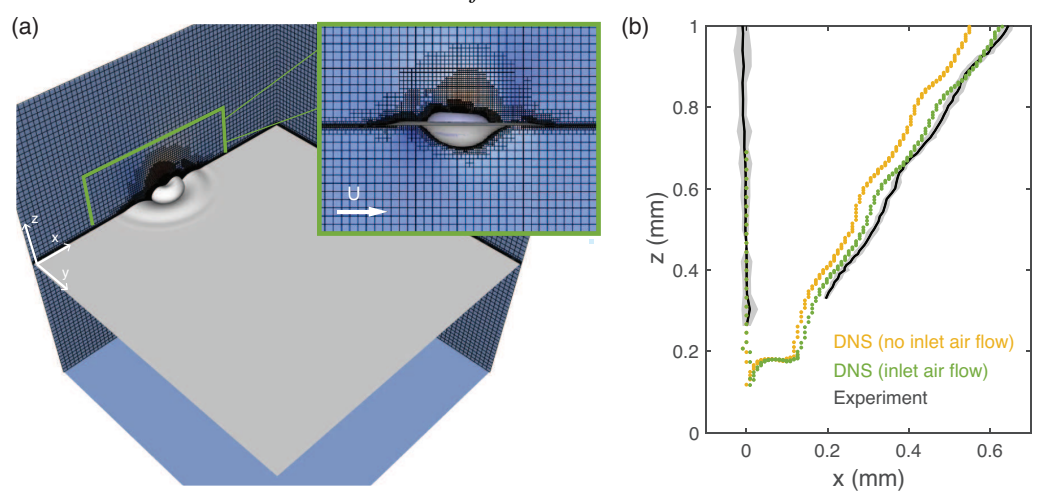


Figure 2. (a) Three-dimensional computational domain, with adaptive mesh highlighted in the inset. Supplementary videos of representative test cases (impact onto both static and moving pools) are also made available as Supplementary Movies 2 and 3. (b) Trajectory of highest point of droplet in the symmetry plane for a case of a 2 cSt silicone oil droplet with R = 0.23 mm, V = 60.3 cm/s, and U = 15 cm/s. Yellow markers are predictions without inlet airflow, green markers are predictions with uniform inlet airflow, and solid lines are experimental measurements. The shaded region represents two standard deviations across experimental trials.

setup. Inflow boundary conditions (and in particular a non-zero horizontal velocity in x) are employed across one face of the cube, with free-slip and impermeability prescribed at the bottom of the geometry, and outflow conditions on all other boundaries. The noted uniform directional horizontal velocity field is prescribed in both pool and gas regions, replicating a fully developed flow near the rotating table liquid-gas surface. Ensuring the gas region has a non-zero velocity was found to be crucial for good agreement with experiments in scenarios in which the horizontal velocity of the pool was non-negligible ($\geq 10\%$) relative to the vertical drop velocity, as showcased in Figure 2(b).

The setup described above, equipped with a mesh refinement strategy based on the position of the liquid-gas interfaces, as well as changes in magnitude of velocity components and vorticity, leads to tractable configurations with $O(10^6)$ computational grid cells, which are executed over 20 dimensionless time units (typically equivalent to $O(10^{-2})$ s in dimensional terms). This can be achieved in approximately 2000 – 3000 CPU hours for each run, executed on local high performance computing clusters over 8-16 CPUs. Following careful verification and previous investigations (Alventosa et al. 2023), we found that a minimum cell size measuring $O(1) \mu m$ (typically 4.49 μm when using 2^{10} grid cells per dimension as the most refined cell size) is sufficient to ensure mesh-independent results in the target metrics. This resolution is also well aligned with previous entrapped gas film measurements in this regime (Tang et al. 2019), albeit without three-dimensional flow features. Few comprehensive numerical studies have been considered in full threedimensional setups given the high numerical cost, however there are excellent examples in both bouncing (Ramírez-Soto et al. 2020) and splashing (Wang et al. 2023) contexts, with the authors highlighting the considerable resources required to fully resolve the features of interest in the target regimes across a sufficiently wide section of the parameter space.

In our implementation coalescence between the drop and the pool is prevented at the level of the volume-of-fluid method by construction (similar to the approach in Ramírez-Soto *et al.* (2020)) to avoid artificial merging that could disrupt the bouncing

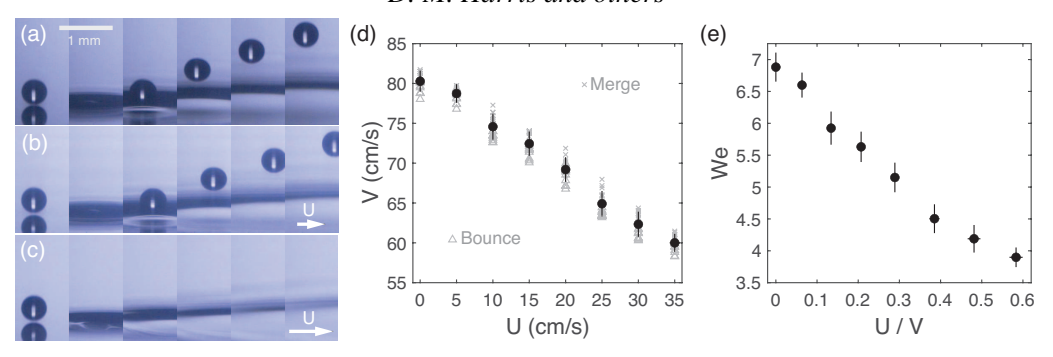


Figure 3. Droplets (2 cSt silicone oil) of radius $R=0.230\pm0.006$ mm with incident vertical speed V impact a fluid bath moving with horizontal speed U. (a-c) Fixed impact velocity $V=73.1\pm1.0$ cm/s with increasing bath speed. Successive images in each sequence are spaced 1/750 seconds apart. Bouncing is observed for (a) U=0 cm/s and (b) U=10 cm/s, with merging at (c) U=20 cm/s. Corresponding videos available in Supplementary Movie 4. (d) Bouncing to coalescence transition as a function of bath speed. Gray triangles are trials where bouncing was observed, gray \times s are trials where coalescence was observed, and black markers are the mean transition values at each bath speed. (e) Critical We as a function of normalized bath speed U/V. In all cases error bars represent propagated error, including one standard deviation across trials.

dynamics. With careful mesh adaptivity, this approach yields mesh-independent results but cannot naturally capture coalescence, which would require sub-continuum physics considerations (Lewin-Jones *et al.* 2024). Instead, we use our numerical infrastructure to probe bouncing regimes identified experimentally, providing mechanistic insight and enabling detailed analysis of rebound dynamics and air layer evolution in this delicate regime.

4. Results

Consistent with what is known from prior work on axisymmetric impacts (and showcased in Figure 1(c,d), for a given set of parameters, there is a critical vertical impact velocity V at which the behavior transitions from bouncing to merging. The goal of the present work is to explore how the introduction of translational bath speed U influences this critical velocity. An experimental sequence is shown in Figure 3, where now the vertical velocity is fixed, and the bath speed is increased incrementally. At U=0 cm/s, the droplet rebounds in an axisymmetric manner, as expected. For U = 10 cm/s, the droplet also successfully rebounds, but departs the surface with a non-zero horizontal velocity bestowed onto it by the bath. However, as the speed is increased further to U = 20 cm/s, merging ensues, suggesting that the bath motion has introduced new conditions favorable to air layer drainage. For fixed droplet size and fluid parameters, this effect is explored systematically in Figure 3(d). Individual trials for the bouncing and merging threshold are shown as the gray markers, with the combined data summarized by the black markers. As can clearly be seen, the bath motion U leads to a systematic reduction in the necessary vertical velocity required to initiate merging. The non-dimensionalized version is presented in Figure 3(e), again highlighting this monotonic trend.

As reviewed in the introduction, the persistence of the intervening air layer determines the impact outcome. As such, our experimental observations suggest that the evacuation of the air layer is enhanced by the motion of the bath. To elucidate the physical mechanism underlying this conclusion, we turn to our companion numerical simulations. In Figure 4(a), the thickness of the air layer in the symmetry plane is plotted as it evolves in time for a representative bouncing case with and without bath motion. For the case of U = 0, the

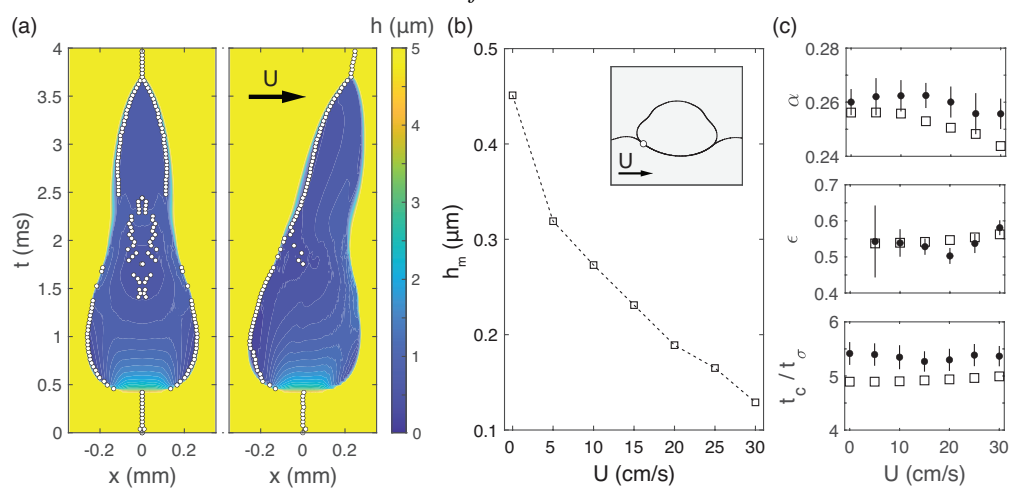


Figure 4. Simulation results of droplets (2 cSt silicone oil) of radius R=0.23 mm with incident vertical speed V=60.3 cm/s impacting a fluid bath moving with horizontal speed U. (a) Evolution of air layer thickness profile along symmetry plane for the case of U=0 (left) and U=15 cm/s (right). Circular markers indicate the point of minimum thickness, which systematically occurs on the upstream side of the contact region for U>0. (b) Minimum air layer thickness as a function of bath speed U. Inset shows a typical slice from the simulation, with the circular marker indicating the position of minimum thickness. (c) Vertical coefficient of restitution (α) , horizontal coefficient of restitution (ϵ) , and non-dimensional contact time (t_c/t_σ) as a function of U for simulations (\Box) and experiments (\bullet) . t_σ is the inertio-capillary timescale defined as $\sqrt{\rho R^3/\sigma}$. For experimental data, error bars represent propagated error, including one standard deviation across trials.

air layer evolves symmetrically, as expected, with the minimum air gap thickness (denoted by the circular markers) occurring on the rim of the contact region for most of the contact period. Introducing bath motion breaks this symmetry, and in particular, the location of minimum thickness now systematically occurs on the upstream edge of the contact region. Figure 4(b) shows the absolute minimum thickness as a function of bath speed, demonstrating that the introduction of bath speed also decreases the minimum thickness, consistent with our conclusion that the horizontal motion must enhance air layer drainage locally, favoring merging behavior. We note that the reported minimum air gap thickness occurs at a sub-grid cell lengthscale, thereby requiring a robust post-processing algorithm to ensure that the extracted value is free from numerical interfacial reconstruction errors, is maintained for a sufficiently long timescale to be reliable, and is standardized across different test cases. An imposed criterion of the air layer thickness being extracted using a rolling window characterized by a lengthscale of at least 5 adjacent contact grid cells and sustained over 10% of the contact time was found to provide a suitable balance between avoiding numerically-induced artifacts in both space and time, and capturing the defining features of the different stages of the rich bouncing dynamics. With these considerations, as depicted in the inset of Figure 4(b), we find that the depression created by the droplet during impact is pressed against the tilted upstream side of the droplet as the bath continues to translate, and is the mechanism responsible for the enhanced drainage. Although not a primary objective of the article, we also present typical bouncing metrics (coefficients of restitution and contact time) for these parameters in Figure 4(c), demonstrating that these factors are largely unaffected by the bath motion. In particular, the contact time is essentially constant with U, suggesting that the 3D-nature of the interaction is responsible for the enhanced drainage, rather than simply a result of a prolonged interaction.

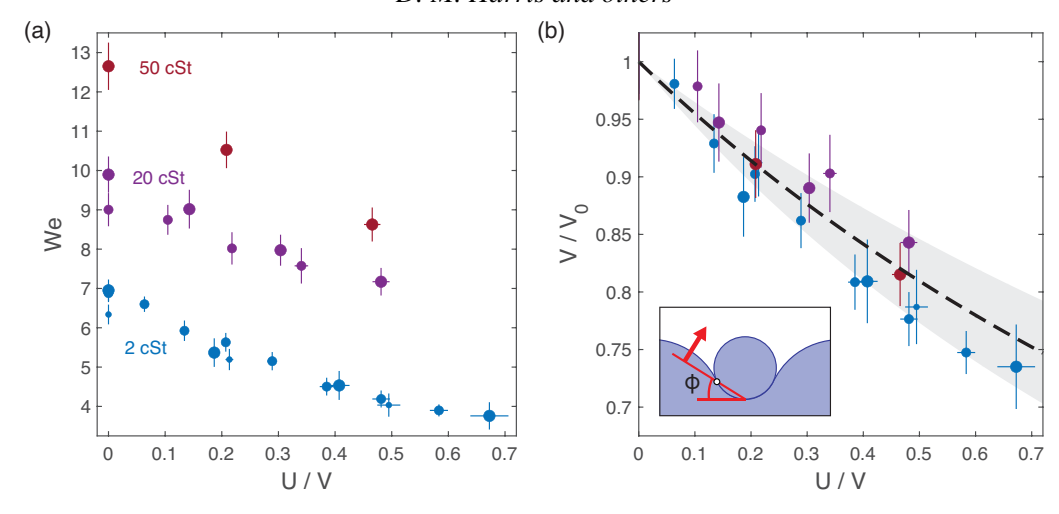


Figure 5. (a) Bouncing to coalescence transition for silicone oil droplets of different viscosities (marker color) and radii (marker size) as a function of the normalized bath speed. For 2 cSt oil (blue): small, medium, and large markers correspond to $R = 0.169 \pm 0.008$, 0.230 ± 0.006 , and, 0.403 ± 0.008 mm, respectively. For 20 cSt oil (purple): medium and large markers correspond to $R = 0.208 \pm 0.009$ and 0.398 ± 0.008 mm, respectively. For 50 cSt oil (red): large markers correspond to $R = 0.443 \pm 0.016$ mm. (b) Critical vertical velocity V normalized by the critical velocity for a still bath V_0 (i.e. with U = 0) under otherwise equivalent conditions. Dashed line (and shaded region) shows equation 4.1 with film angle parameter $\phi = 25.2 \pm 5.2^{\circ}$. In all cases error bars represent propagated error, including one standard deviation across trials.

Lastly, we explore the generality of our main finding: that the normal Weber number for the bouncing to coalescence transition decreases with relative bath motion. Figure 5(a) presents the results for the critical impact Weber number as a function of normalized bath speed for multiple droplet sizes and viscosities (up to 50 cSt). While the threshold is only weakly sensitive to droplet size, there is a clear influence of viscosity, consistent with prior axisymmetric results (Tang et al. 2018). Nevertheless, in every parameter combination explored herein, the critical We systematically decreases with bath speed. If we replot the data for the critical vertical velocity V, normalized by the axisymmetric critical velocity V_0 (for U=0) in each case, all of the collected data nearly collapses along a single curve in Figure 5(b). This collapse, which involves only kinematic parameters of the problem, suggests a geometric interpretation of our result. As discerned from the simulation, the tilted upstream contact surface and the relative bath motion conspire to promote upstream air layer drainage. If one then assumes air layer evacuation is caused by the normal projection of both V and U onto a titled surface with angle ϕ (see inset of Figure 5(b)), a new characteristic velocity for the transition can be defined as $V_c = V \cos \phi + U \sin \phi$. When U = 0, $V_c = V_0 \cos \phi$, and we can find

$$\frac{V}{V_0} = \frac{1}{1 + \frac{U}{V} \tan \phi}. (4.1)$$

Fitting the best value of ϕ to each dataset yields $\phi = 25.2 \pm 5.2^{\circ}$, which is consistent with the typical average film slopes observed in our simulations and those of Lewin-Jones (2024) for the axisymmetric scenario. While the details of the gas film evolution are dynamic and complex, our combined results nevertheless suggest a simple coherent physical picture. The deformation of the bath caused by the droplet impact itself leads to a tilted mediating air film, with drainage on the upstream side then enhanced by the relative bath motion.

Crudely approximating the substrate as a tilted planar surface with angle $\phi \approx 25^{\circ}$ allows us to rationalize the collapse of all our data, motivated by this simple geometric understanding of the underlying physical mechanism at play.

5. Discussion

Despite the progress presented herein, there are some limitations that should be highlighted and may also serve as motivation for future work. Due to experimental constraints, the study was restricted to scenarios where U < V (corresponding to near-normal impacts in the equivalent oblique problem). It is plausible that higher bath speeds (or shallow impact angles as in Leneweit et al. (2005)) would result in different phenomenology. Furthermore, the present work focuses on millimetric droplets, whereas it has been shown that for the case of both oblique droplet streams and single droplets impacting normally, small droplets $(R \le 100 \,\mu\text{m})$ exhibit an additional coalescence regime that precedes the bouncing regime (Javaratne & Mason 1964; Bach et al. 2004; Zhao et al. 2011; Lewin-Jones 2024). leading to a coalescence-bouncing-coalescence transition sequence as the Weber number is increased from zero. Future work on the topic might also explore the role of layer depth (Pan & Law 2007), charge (Jayaratne & Mason 1964), differing drop and bath fluids (Wu & Saha 2022), ambient gas properties (Schotland 1960), wind (Liu 2018), curved interfaces (such as sessile droplets (Moon et al. 2018)), or unsteady fluid interfaces (Couder et al. 2005; Che et al. 2015). From the modeling perspective, additional work extending the hybrid open-source computational framework of Sprittles (2024) and Lewin-Jones (2024) to 3D would provide additional physical insight and a predictive capability currently unavailable for this highly multiscale problem.

Supplementary Material. Supplementary movies are available in the associated repository.

Funding. The authors gratefully acknowledge the financial support of the National Science Foundation (NSF CBET-2123371) and the Engineering and Physical Sciences Research Council (EPSRC EP/W016036/1).

Declaration of Interests. The authors report no conflict of interest.

Data availability. The DNS implementation, as well as associated data pre- and post-processing scripts are made available at https://github.com/rcsc-group/BouncingDropletsMovingPool3D. Data is available from the corresponding author upon request.

REFERENCES

- ALVENTOSA, L.F.L., CIMPEANU, R. & HARRIS, D.M. 2023 Inertio-capillary rebound of a droplet impacting a fluid bath. *Journal of Fluid Mechanics* **958**, A24.
- BACH, G.A., KOCH, D.L. & GOPINATH, A. 2004 Coalescence and bouncing of small aerosol droplets. *Journal of Fluid Mechanics* **518**, 157–185.
- Castrejón-Pita, J.R., Muñoz-Sánchez, B.N., Hutchings, I.M. & Castrejón-Pita, A.A. 2016 Droplet impact onto moving liquids. *Journal of Fluid Mechanics* 809, 716–725.
- Che, Z., Deygas, A. & Matar, O.K. 2015 Impact of droplets on inclined flowing liquid films. *Physical Review E* **92** (2), 023032.
- Ching, B., Golay, M.W. & Johnson, T.J. 1984 Droplet impacts upon liquid surfaces. *Science* 226 (4674), 535–537.
- Couder, Y., Fort, E., Gautier, C.-H. & Boudaoud, A. 2005 From bouncing to floating: noncoalescence of drops on a fluid bath. *Physical Review Letters* **94** (17), 177801.
- DOAK, W.J., LAIACONA, D.M., GERMAN, G.K. & CHIAROT, P.R. 2016 Rebound of continuous droplet streams from an immiscible liquid pool. *Physics of Fluids* 28 (5).
- Gauthier, A., Bird, J.C., Clanet, C. & Quéré, D. 2016 Aerodynamic Leidenfrost effect. *Physical Review Fluids* 1 (8), 084002.
- HARRIS, D.M., LIU, T. & BUSH, J.W.M. 2015 A low-cost, precise piezoelectric droplet-on-demand generator. Experiments in Fluids **56**, 1–7.
- Huang, Q. & Zhang, H. 2008 A study of different fluid droplets impacting on a liquid film. *Petroleum Science* 5 (1), 62–66.
- ILLARI, L., MARSHALL, J., BANNON, P., BOTELLA, J., CLARK, R., HAINE, T., KUMAR, A., LEE, S., MACKIN, K.J., McKinley, G.A., Morgan, M., Najjar, R., Sikora, T. & Tandon, A. 2009 Weather in a tank. Bulletin of the American Meteorological Society 90 (11), 1619–1632.

- IONKIN, N. & HARRIS, D.M. 2018 Note: A versatile 3D-printed droplet-on-demand generator. Review of Scientific Instruments 89 (11).
- JAYARATNE, O.W. & MASON, B.J. 1964 The coalescence and bouncing of water drops at an air/water interface. *Proc. R. Soc. Lond. A* **280** (1383), 545–565.
- Leneweit, G., Koehler, R., Roesner, K.G. & Schäfer, G. 2005 Regimes of drop morphology in oblique impact on deep fluids. *Journal of Fluid Mechanics* **543**, 303–331.
- Lewin-Jones, P. 2024 Liquid drop impacts: when trapped gas nanofilms lead to bouncing. PhD thesis, University of Warwick.
- Lewin-Jones, P., Lockerby, D.A. & Sprittles, J.E. 2024 Collision of liquid drops: bounce or merge? *Journal of Fluid Mechanics* **995**, A1.
- Liu, X. 2018 Experimental study of drop impact on deep-water surface in the presence of wind. *Journal of Physical Oceanography* 48 (2), 329–341.
- Moon, J.H., Choi, C.K., Allen, J.S. & Lee, S.H. 2018 Observation of a mixed regime for an impinging droplet on a sessile droplet. *International Journal of Heat and Mass Transfer* **127**, 130–135.
- Neitzel, G.P. & Dell'Aversana, P. 2002 Noncoalescence and nonwetting behavior of liquids. *Annual Review of Fluid Mechanics* **34** (1), 267–289.
- PAN, K.-L. & LAW, C.K. 2007 Dynamics of droplet-film collision. Journal of Fluid Mechanics 587, 1-22.
- PHILLIPS, KA, CIMPEANU, R & MILEWSKI, PA 2025 Modelling two-dimensional droplet rebound off deep fluid baths. *Proceedings of the Royal Society A* **481** (2317), 20240956.
- POPINET, S. 2009 An accurate adaptive solver for surface-tension-driven interfacial flows. *Journal of Computational Physics* **228** (16), 5838–5866.
- POPINET, S. 2015 A quadtree-adaptive multigrid solver for the Serre-Green-Naghdi equations. *Journal of Computational Physics* **302**, 336–358.
- Ramírez-Soto, O., Sanjay, V., Lohse, D., Pham, J.T. & Vollmer, D. 2020 Lifting a sessile oil drop from a superamphiphobic surface with an impacting one. *Science Advances* **6** (34), eaba4330.
- RAY, S., HAN, Y., YUE, Z., GUO, H., CHAO, C. Y. H. & CHENG, S. 2024 New insights into head-on bouncing of unequal-size droplets on a wetting surface. *Journal of Fluid Mechanics* **983**, A25.
- RAYLEIGH 1899 XXXVI. investigations in capillarity. The London, Edinburgh, and Dublin Philosophical Magazine and Journal of Science 48 (293), 321–337.
- REIN, M. 1993 Phenomena of liquid drop impact on solid and liquid surfaces. Fluid Dyn. Res 12 (2), 61-93.
- RODRIGUEZ, F. & MESLER, R. 1985 Some drops don't splash. J. Colloid Interface Sci. 106 (2), 347-352.
- Sanjay, V., Chantelot, P. & Lohse, D. 2023 When does an impacting drop stop bouncing? *Journal of Fluid Mechanics* **958**, A26.
- Schotland, R.M. 1960 Experimental results relating to the coalescence of water drops with water surfaces. *Discussions of the Faraday Society* **30**, 72–77.
- Sprittles, J.E. 2024 Gas microfilms in droplet dynamics: When do drops bounce? *Annual Review of Fluid Mechanics* **56** (1), 91–118.
- Tang, X., Saha, A., Law, C.K. & Sun, C. 2016 Nonmonotonic response of drop impacting on liquid film: mechanism and scaling. *Soft Matter* **12** (20), 4521–4529.
- Tang, X., Saha, A., Law, C.K. & Sun, C. 2018 Bouncing-to-merging transition in drop impact on liquid film: Role of liquid viscosity. *Langmuir* **34** (8), 2654–2662.
- Tang, X., Saha, A., Law, C.K. & Sun, C. 2019 Bouncing drop on liquid film: dynamics of interfacial gas layer. *Physics of Fluids* **31** (1).
- Thrasher, M., Jung, S., Pang, Y.K., Chuu, C.-P. & Swinney, H.L. 2007 Bouncing jet: A newtonian liquid rebounding off a free surface. *Physical Review E* **76** (5), 056319.
- Wang, H., Liu, S., Bayeul-Lainé, A.-C., Murphy, D., Katz, J. & Coutier-Delgosha, O. 2023 Analysis of high-speed drop impact onto deep liquid pool. *Journal of Fluid Mechanics* **972**, A31.
- Wu, X. & Saha, A. 2022 Droplet impact on liquid films: Bouncing-to-merging transitions for two-liquid systems. *Physics of Fluids* **34** (10).
- Wu, Z., Hao, J., Lu, J., Xu, L., Hu, G. & Floryan, J.M. 2020 Small droplet bouncing on a deep pool. *Physics of Fluids* 32 (1).
- Yarin, A.L. 2006 Drop impact dynamics: splashing, spreading, receding, bouncing. . . . *Annual Review of Fluid Mechanics* **38** (1), 159–192.
- Zhao, H., Brunsvold, A. & Munkejord, S.T. 2011 Transition between coalescence and bouncing of droplets on a deep liquid pool. *International Journal of Multiphase Flow* 37 (9), 1109–1119.
- Zhbankova, S.L. & Kolpakov, A.V. 1990 Collision of water drops with a plane water surface. *Fluid Dynamics* **25** (3), 470–473.
- ZOU, J., WANG, P.F., ZHANG, T.R., FU, X. & RUAN, X. 2011 Experimental study of a drop bouncing on a liquid surface. *Physics of Fluids* 23 (4).